Infima statistics of entropy production in an underdamped Brownian motor

Ke Cheng,[1] Jia-Qi Dong,[2,1] Wen-Hui Han,[1] Fei Liu [ID],[3] and Liang Huang [ID][1,*]

[1]*School of Physical Science and Technology, and Key Laboratory for Magnetism and Magnetic Materials of MOE,
Lanzhou University, Lanzhou, Gansu 730000, China*
[2]*Institute of Theoretical Physics, CAS, Beijing 100190, China*
[3]*School of Physics, Beihang University, Beijing 100191, China*

The second law of thermodynamics states that the entropy never decreases for isolated macroscopical systems, which defines the arrow of time. For small systems, although the entropy increases on average, due to strong fluctuation, it may encounter a temporary decrease. The probability of negative entropy production follows the fluctuation theorem. Recently, it has been demonstrated theoretically the infima law that there exists a lower bound for the average values of the minima of the negative entropy production, which is $-k_B$. In this paper, we have constructed a horizontal Brownian motor immersed in a granular gas, whose dynamics is governed by the underdamped stochastic process. By recording the angular motion of the motor and measuring the key parameters of the system, we experimentally demonstrate that, despite the nonideal elements in the experiments and that the complex underlying dynamics, the average value of the minima of the negative entropy production is still bounded by $-k_B$, which may invoke further theoretical investigations of the applicability of the infima law in nonideal realistic small systems.

I. INTRODUCTION

The second law of thermodynamics infers the irreversibility of natural processes in isolated macroscopic systems, where in general the total entropy of the system is a nondecreasing quantity. For mesoscopic and microscopic systems, or equivalently macroscopic but small systems [1] such as the granular gases, the scale of fluctuation can be large and results in temporarily decrease of the total entropy or a negative entropy production. It has been found that such negative entropy productions follow the fluctuation theorem [2–7], which can be regarded as a microscopic description of the second law of thermodynamics. It states that the ratio between the probability of a positive total entropy production ΔS_{tot} and that for a negative one but with the same amplitude will be an exponential function of ΔS_{tot} in a finite time duration,

$$\frac{P(\Delta S_{\text{tot}})}{P(-\Delta S_{\text{tot}})} = e^{\Delta S_{\text{tot}}/k_B}, \tag{1}$$

where k_B is the Boltzmann constant. There are numerous experimental or numerical tests that verified the fluctuation theorem, including granular matter [8–13], harmonic oscillator [14,15], optical trap [16,17], circuit systems [18–21], RNA folding experiment [22], and optomechanical systems [23], etc.

Fluctuations of entropy production lead to a fundamental question: Will there be a minimum value of negative entropy production? A recent work [24] by Neri *et al.* provided an affirmative answer for nonequilibrium steady processes. They defined the infimum entropy production in a time duration

t_L as $S_{\text{inf}}(t_L) = \inf_{0 \leqslant t' \leqslant t_L} S_{\text{tot}}(t')$, and by assuming that the entropy production in a nonequilibrium state is martingale, they found that the distribution of the negative entropy production is exponential when t_L is large and the average value of this negative infimum satisfies

$$\langle S_{\text{inf}}(t_L) \rangle \geqslant -k_B, \tag{2}$$

where the condition of equality is $t_L \to \infty$. This infima law circumscribes the variation of entropy: No matter how fast the entropy production rate is, the mean value of the global infimum is always larger than $-k_B$.

Very recently, Singh *et al.* investigated the infima law of the negative fluctuations of stochastic entropy production in an electronic double-dot system [25], verified that for different parameter values, the average value of the minima of the negative entropy production always lie above $-k_B$. The double dot structure enables the measurement of the direction of single-electron currents, which is key to measure the entropy production. Though the apparatus in the experiment is sophisticated enough to measure the single-electron charging effect, the dynamics is rather simple that the system contains only four allowable states and the dynamics is governed by the master equation describing the hopping processes between these states. Theoretically, Neri *et al.* examined a simple overdamped drift-diffusion model with periodic boundary condition. Due to the simplicity of the dynamics, the extreme value problem of the entropy production was obtained analytically, and the infima law has been corroborated [24]. In addition, the extreme value problem of the entropy production has also been obtained analytically for general, multidimensional, overdamped Langevin processes [26]. The overdamped model is popular in exploring

*huangl@lzu.edu.cn

dynamical and thermodynamic properties of nonequilibrium small systems [24,27–30].

However, realistic systems may be far from the overdamped limit. For example, the electronic circuit system [19–21], the diffusion of drugs [31], and the Brownian motor immersed in a granular gas [9] are all described by the underdamped equation. For underdamped systems, the most significant difference from the overdamped system is the impact of inertia, resulting in nontrivial exponential velocity correlations, leading to distinct diffusion dynamics. In contrast, for overdamped Langevin systems, the motion is completely dominated by the white noise, hence it is delta correlated. Our interest is thus in such realistic systems with underdamped stochastic processes and nonideal situations presented in the experiment, will this infima law still hold? Our results using the underdamped granular Brownian motor provide an affirmative answer. Therefore, despite the remarkable inherent difference between underdamped and overdamped dynamics and in the presence of all kinds of nonidealities, they seem to follow the same infima law [24]. This may invoke further investigations of the applicable range of theories in realistic nonideal small systems.

The rest of this paper is organized as follows. In Sec. II, the experimental setup of the Brownian motor in a granular gas is articulated, and the Langevin equation is adopted to describe the dynamics of the motor. Section III calculates the total entropy production ΔS using two different procedures to cross-validate the results and demonstrates that the total entropy production satisfies the fluctuation theorem reasonably well, with deviations when $|\Delta S|$ is large. Section IV shows the infima statistics of the total entropy, that for the parameter range where the calculations and statistics are valid, the infima law is well satisfied. Discussions and conclusion are provided in Sec. V.

II. THE BROWNIAN MOTOR

A. Experimental setup

Following the pioneering experimental setups for granular Brownian motor [11,32–38], we have carried out a systematic experimental investigation of the infima law of the total entropy production in a granular Brownian motor. Figure 1 shows the schematic diagram of the experiment. A Brownian motor made of resin is immersed in a driven granular gas [9,35] in a circular container with a height of 2.5 cm and diameter $d = 18.0$ cm. The granular materials are plastic balls with a 6 mm diameter, and there are $N = 224$ particles in the container. The resulting filling rate, i.e., the ratio of the area occupied by the granular particles and the area of the container, is 0.2489. The container is fixed on a vibration table (V.T.) that can vibrate vertically in the frequency range from 2 to 1000 Hz. In the experiment, the frequency of vibration is fixed at 100 Hz and the amplitude is set to 0.15 mm. Note that although the V.T. is set to vibrate vertically, it may have nonnegligible horizontal vibration motion. To be concrete, we have measured the horizontal motion via a laser rangefinder, and found that the amplitude of the horizontal vibration is about 1.5 μm, which is only about 1% of the vertical vibration. Thus the horizontal motion of the V.T. can almost be
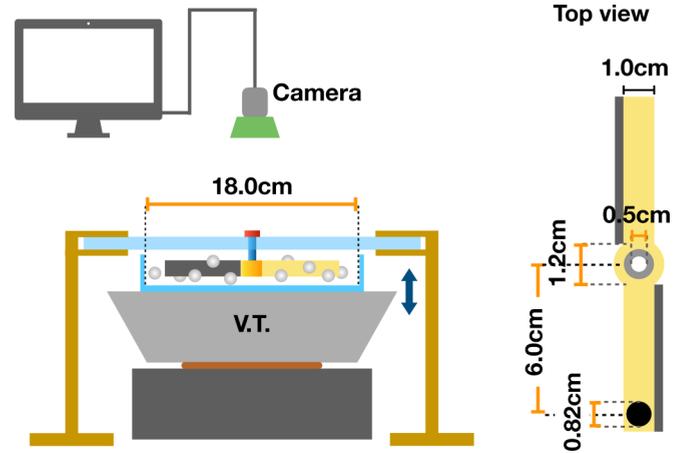

FIG. 1. The experimental setup. The Brownian motor with a circular tracking mark (the black point on the motor) is fixed on the floating cover. The vibration table (V.T.) supplies vertical sinusoidal vibration and maintains the steady granular gas state. The vibration amplitude is 0.15 mm, and the frequency is 100 Hz. The distance between the center of the motor and the center of the mark point is $l_m = 6.0$ cm, and the diameter of the container is $d = 18.0$ cm.

neglected and is not likely to introduce observable effects to the motor system. In addition, here the exact values of the vibrator parameters such as the vibration frequency and the amplitude are irrelevant to our main findings insofar as the granular gas state is maintained steadily. The motor has two paddles with 1.0 cm in both width and height. Its center is connected by a ball-bearing and a shaft to the cover of the container which is isolated from the V.T. and is static during the experiment. Two opposite-side surfaces of the paddles are attached with rubber tapes to break the symmetry, as shown in Fig. 1. The collision coefficient is different, which is smaller for the side with the rubber tape. Due to the conservation of momentum, the collision of the particles to the side with rubber tapes transfers a smaller momentum to the motor than that to the other side, leading to a net force on average from the other side to the side with the rubber tape. Therefore, under the collision from the particles, this asymmetry results in a fluctuated drift motion of the motor.

There is a black point with a diameter of 8.2 mm at the end of one paddle to mark the angular position of the motor, which is larger than the plastic balls and can be easily recognized. The length between the center of the motor and the center of the mark is $l_m = 6.0$ cm. A high-speed complementary metal oxide semiconductor camera (Basler, acA2040-180 km) on the top of the vibration table is used to capture the state of the motor, and we use the ImageJ software [39] to acquire the position of the black mark for each frame. Then we can obtain the trajectory of the black mark, and henceforth the angle $\theta(t)$ of the motor at each time instance t. This method can avoid touching the motor when measuring the motor's position, which could prevent additional friction. The angular velocity $\omega(t)$ can thus be approximated as $[\theta(t + t_f) - \theta(t)]/t_f$, where t_f is the time elapsed between two adjacent frames. To be specific, after tracking the position $(x(t), y(t))$ of the center of the black mark on the Brownian motor relative to the motor's center, after some algebra, the angular velocity is
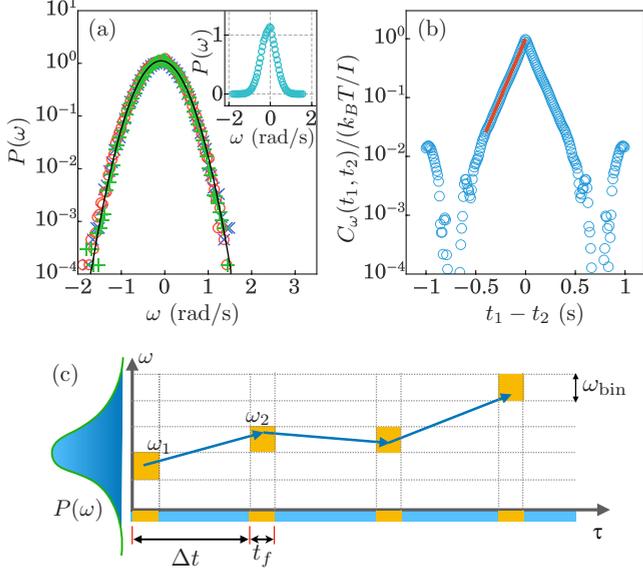
FIG. 2. (a) The distributions of angular velocity. The red circles are the distribution for $0 < t \leqslant 3 \times 10^6$ frames, the green pluses for $t = 3 \times 10^6 < t \leqslant 6 \times 10^6$, and the blue crosses for $6 \times 10^6 < t \leqslant 9 \times 10^6$. All of the three distributions are Gaussian and coincide with each other well. The curve is Eq. (9) with parameter values derived from the experiments. Inset shows the distribution for all the data in the linear scale, where the asymmetry for ω to $-\omega$ is clear. The mean and the standard deviation of ω is -0.087 rad/s and 0.356 rad/s, respectively. (b) The autocorrelation function for $\omega(t)$. The slope of the red line indicates the characteristic time of the Brownian motor: $\tau = |1/\text{slope}| = 0.112$ s. (c) The sampling method for this experiment. The yellow blocks indicate discretization of ω. The time duration between two adjacent ω_is $(i = 1, 2)$ is Δt.

approximately

$$\omega(t) \approx \frac{1}{t_f}\arcsin\frac{1}{l_m^2}[x(t)y(t + t_f) - x(t + t_f)y(t)].$$

Note that the angular velocity should be the instantaneous value. To approximate the instantaneous angular velocity, the frame rate of the camera should be as high as possible. In our experiment, the frame rate is 500 fps, leading to a time duration between two frames $t_f = 2$ ms. The exposure time of a single frame is $t_e = 0.5$ ms to ensure that the camera can record the position of the mark with a high precision. We have recorded 5 h of data in the experiment, which has in total 9×10^6 frames. Figure 2(a) plots the distribution of the values of ω in three different time segments: $0 \rightarrow 3 \times 10^6$ frames, $3 \times 10^6 \rightarrow 6 \times 10^6$ frames, and $6 \times 10^6 \rightarrow 9 \times 10^6$ frames. It is clear that they all follow the same Gaussian distribution, thus the system is stationary and the results are stable during the time of recording.

B. The Langevin equation and the key parameters

The motion of the asymmetric Brownian motor can be described with the underdamped Langevin equation:

$$\frac{d}{dt}\omega(t) = -\frac{\gamma}{I}\omega(t) + \frac{M}{I} + \eta(t),\tag{3}$$

where I is the moment of inertia, γ is the coefficient of viscosity, and $\omega(t)$ is the angular velocity. Note that here the trajectory is the time series of the angular velocity. M stands for the constant torque of the averaging effect of the collisions from the granular particles to the asymmetric motor. $\eta(t)$ is a Gaussian white noise due to the fluctuation of the collision, which follows the fluctuation-dissipation theorem [40,41],

$$\langle \eta(t)\eta(t')\rangle = 2D\delta(t - t'),\tag{4}$$

where $D = k_B T \gamma / I^2$ and T is the motor's effective kinetic temperature which can be obtained as $T = I(\langle \omega^2 \rangle - \langle \omega \rangle^2)/k_B$. Note that although the results are insensitive to the detailed parameter values, the vibration frequency, amplitude, and the number of granular particles should be in a proper range that the granular particles are maintained in a gaseous state and the collisions with the motor are frequent, to guarantee that $\eta(t)$ can be approximated well by the Gaussian white noise (see Appendix A). The moment of inertia I is measured by a torsional pendulum, which is $I = (3.505 \pm 0.008) \times 10^{-5}$ kg m^2. Our experimental measurement yields $\langle \omega^2 \rangle = 0.134$ rad^2/s^2, and the mean drift speed $\langle \omega \rangle = -0.087$ rad/s, as the motor rotates in a counterclockwise direction. The temperature of the Brownian motor is thus $T = 4.45 \times 10^{-3}$ mJ/k_B. The granular temperature is measured as well with a tracer particle that is painted with a different color. The mass of the particle is $m = 1.284 \pm 0.003$ g, and the measured mean square velocity is $\langle v^2 \rangle = 7.36 \times 10^{-3}$ m^2/s^2, yielding a temperature of the granular environment $T_g = 4.72 \times 10^{-3}$ mJ/k_B. The motor's effective temperature T is a little bit lower than that of the granular gas T_g as the collision between the granular particle and the motor is not ideally elastic. Note that T and T_g are the effective kinetic temperature of the Brownian motor and the granular gases, respectively. They are not related with the actual room temperature. Since the motor's effective temperature T is accompanied with the entropy, the precision of its value will be critical for determining the entropy. This requires that in measuring the angular velocity $\omega(t)$, the time interval should be minimum. In our case, it is t_f, which is only 2 ms.

If the Gaussian white noise is ignored, then Eq. (1) has an analytical solution: $\omega(t) = \langle \omega \rangle + \omega_0 \exp[-t/\tau]$, where $\langle \omega \rangle = M/\gamma$, $\langle \omega \rangle + \omega_0$ is the initial angular velocity, which is typically zero as the system starts from the static state, and $\tau = I/\gamma$ is the characteristic time of the system. To determine τ, it is noted that the autocorrelation time of a Brownian motion has the form [41]:

$$C_\omega(t_1, t_2) = \langle \omega(t_1)\omega(t_2)\rangle = \frac{k_B T}{I}e^{-|t_1 - t_2|/\tau}.\tag{5}$$

It is convenient to normalize the function C_ω and plot in the logarithmic scale, then the slope of the fitting to the data yields $\pm 1/\tau$. To be specific, the red fitting line in Fig. 2(b) indicates that the characteristic time of the system is $\tau = 0.112$ s [42].

III. THE TOTAL ENTROPY PRODUCTION AND THE FLUCTUATION THEOREM

A. The total entropy production

In the experiment, the asymmetric motor is immersed in the granular bath, which provides an external torque M (exerting

work into the motor), noise $\eta(t)$, and also the friction due to the random collisions. Note that for the motor system the ball-bearing introduces an additional friction force, small but finite. Although it can be neglected in our case as it is one order smaller than that from the collision with the granular particle, it could be crucial when the granular particles are less dense.

Since the motor only has a rotational degree of freedom, it is equivalent to a one-dimensional particle with a biased random driven force, providing external work and energy fluctuations to the particle, which then flows to the thermal bath. As the whole system is composed of the motor and the granular environment, the total entropy production ΔS_{tot} equals to a sum of the entropy production of the motor ΔS_{sys} and the entropy production of the environment ΔS_{env} due to the motor [28], that is,

$$\Delta S_{\text{tot}} = \Delta S_{\text{env}} + \Delta S_{\text{sys}}, \qquad (6)$$

where

$$\Delta S_{\text{sys}} = k_B \ln[P(\omega_0)/P(\omega_1)] \qquad (7)$$

is the Gibbs entropy change of the motor and ω_0 and ω_1 are the states of the system at given two time instances, t_0 and t_1.

The distribution of the angular velocity in the system entropy production ΔS_{sys} can be counted from the measured data. Alternatively, it can be obtained analytically, as follows. The corresponding Fokker-Planck equation of the Langevin equation (3) is

$$\frac{\partial P(\omega, t)}{\partial t} = -\frac{\partial}{\partial \omega}\Big[\Big(-\frac{\gamma}{I}\omega + \frac{M}{I}\Big)P(\omega, t)\Big]$$
$$+ D\frac{\partial^2}{\partial \omega^2}P(\omega, t), \qquad (8)$$

whose stable solution at t_0 is

$$P(\omega_0) = C\exp\big[\big(-\tfrac{1}{2}I\omega_0^2 + M\tau\omega_0\big)/(k_B T)\big], \qquad (9)$$

where $\omega_0 = \omega(t_0)$, $\tau = I/\gamma$, and C is a normalization constant. At t_1, the probability distribution of $\omega_1 = \omega(t_1)$ has the same form

$$P(\omega_1) = C\exp\big[\big(-\tfrac{1}{2}I\omega_1^2 + M\tau\omega_1\big)/(k_B T)\big]. \qquad (10)$$

Employing Eqs. (9) and (10), we obtain the system entropy

$$\Delta S_{\text{sys}} = \frac{\frac{I}{2}\big[\omega_1^2 - \omega_0^2\big] - M\tau[\omega_1 - \omega_0]}{T}. \qquad (11)$$

For the motor, from t_0 to t_1, one has the first law of thermodynamics $\Delta E_k = \Delta W + \Delta Q$, where $\Delta E_k = \frac{1}{2}I(\omega_1^2 - \omega_0^2)$ is the increased kinetic energy of the motor, $\Delta W = M\int_{t_0}^{t_1}\omega(t)dt = M(\theta_2 - \theta_1)$ is the injected work to the motor by the granular gas, ΔQ is the heat from the environment to the motor. Therefore $-\Delta Q$ is the heat flow from the motor into the granular environment. Thus the environment entropy change due to the motor is given by [9]

$$\Delta S_{\text{env}} = -\Delta Q/T = (\Delta W - \Delta E_k)/T$$
$$= \big[M(\theta_1 - \theta_0) - \tfrac{1}{2}I\big(\omega_1^2 - \omega_0^2\big)\big]/T, \qquad (12)$$

where T is the effective kinetic temperature of the granular environment felt by the motor. From this equation, ΔS_{env} can

be obtained directly from the measured time series of $\theta(t)$ and the derived $\omega(t)$, where the values of the parameters M, I, and the effective temperature T can be deducted from the experimental data. Combining Eqs. (12) and (11), the total entropy production can be written as

$$\Delta S_{\text{tot}} = M\frac{\theta_1 - \theta_0 - \tau(\omega_1 - \omega_0)}{T} \equiv \Delta S_{\text{tot}}^{(\text{I})}. \qquad (13)$$

Here we denote the total entropy production as $\Delta S_{\text{tot}}^{(\text{I})}$, since in the following, we will introduce a different procedure to calculate the total entropy production that only based on counting the angular velocity trajectories.

B. The trajectory-based total entropy production

From Eq. (12), in the calculation of ΔS_{env}, the values of the parameters M, I, and T need to be acquired from the experimental data in advance. Any inaccuracy in evaluating these parameters will cause uncertainty in the estimation of ΔS_{env}. An alternative method is to calculate the trajectory entropy ΔS_{traj} [28], which only needs to count the trajectory of the angular velocity in Eq. (3) and can be a good approximation to the environment entropy ΔS_{env}. This has been demonstrated in a circuit system [21]. In addition, the system entropy [Eq. (7)] can also be counted from the trajectory time series. Thus the total entropy production can be expressed in terms of the angular velocity trajectory only, eliminating possible uncertainties occurred in estimating intermediate parameters.

Concretely, the trajectory entropy is related to the ratio of the probability to observe a forward trajectory $\overrightarrow{\omega}$ and the probability to observe its time-reversed counterpart $\overleftarrow{\omega}$ [28]:

$$\Delta S_{\text{traj}} = k_B \ln\frac{P(\overrightarrow{\omega})}{P(\overleftarrow{\omega})}. \qquad (14)$$

Practically, it is convenient to approximate the trajectory in phase space by a sequence of jumps, i.e., ω_0, ω_1, ..., ω_n, described by Markov processes in discrete time $t_j = j\Delta t$, where j runs from 0 to n with $n\Delta t = t_n$ [43]. The corresponding reverse trajectory is $\tilde{\omega}_j = \hat{T}\omega_{n-j} = -\omega_{n-j}$. Then Eq. (14) becomes

$$\Delta S_{\text{traj}} = k_B \ln\frac{P(\omega_n|\omega_{n-1})\cdots P(\omega_1|\omega_0)}{P(\tilde{\omega}_n|\tilde{\omega}_{n-1})\cdots P(\tilde{\omega}_1|\tilde{\omega}_0)}. \qquad (15)$$

Furthermore, the angular velocity of the Brownian motor is in principle a continuous real number. Strictly speaking, it is almost impossible to acquire a trajectory that is precisely the time-reversed counterpart for a given forward continuous trajectory. Thus, we take a coarse-graining process on angular velocity, i.e., discretize ω using small bins, as shown in Fig. 2(c). The size of the bin should be chosen properly as it will lose much of the details of the angular velocities if the bin is too large, and if the bin is too small, it will decrease the number of corresponding reverse trajectories or even lead to no reverse trajectories for a considerable amount of forward trajectories, rendering unreliable statistics. Both limiting cases will lead to inaccurate results. In the following, the size of the bin is chosen as $\omega_{\text{bin}} \simeq 0.1$ rad/s, which is about 1/20 of the range from the minimum value to the maximum value of the angular velocity.

In Appendix B, following a similar procedure of Ref. [21] and using the analytic solutions of the Fokker-Planck equation (8), for the Brownian motor, we have demonstrated theoretically the equivalence of the two-step trajectory entropy production $\Delta S_{\text{traj}}^{(2)} = k_B \ln[P(\omega_0 \to \omega_1)/P(-\omega_1 \to -\omega_0)]$ and the environment entropy production ΔS_{env} in the small time interval limit. This has also been corroborated directly from the experimental measurements. In addition, we have demonstrated that for multistep trajectory entropy production $\Delta S_{\text{traj}}^{(n)}$, theoretically, it will agree with the environment entropy production even better (see Appendix C). Indeed, the mean values of the two entropy production agree in a larger range of the time interval when the number of steps is larger. But due to the limited data, the statistics for multistep trajectory entropy production is not so sufficient, resulting in a degraded agreement between the specific time series of the trajectory and environment entropy productions. In the following, we choose two-step trajectories, i.e., each trajectory contains only two elements, $[\omega_0, \omega_1]$, where $t_1 = t_0 + \Delta t$ [see Fig. 2(c)], to ensure that there are many enough reverse trajectories for statistics. With these conditions, the fraction of forward trajectories with no reverse counterparts is less than one percents. Note that the transition from ω_0 to ω_1 should be Markovian, which cannot be entirely fulfilled in the experiments. However, when Δt is much larger than the time interval t_f between two adjacent frames, it is still a good approximation (Appendix D). In dealing with the data, Δt is selected from 0.01 s to 0.40 s, while $t_f = 0.002$ s, and the process is approximately Markovian.

Based on the trajectory statistics only, we define

$$\Delta S_{\text{tot}}^{(\text{II})} = \Delta S_{\text{traj}} + \Delta S_{\text{sys}}$$
$$= k_B \ln \frac{P(\omega_1|\omega_0)}{P(-\omega_0|-\omega_1)} + k_B \ln \frac{P(\omega_0)}{P(\omega_1)}. \quad (16)$$

Here we have employed the two-step trajectory entropy. In calculating the trajectory entropy and the system entropy, the probability function can be obtained directly by counting the angular velocity trajectories, thus all quantities in this expression can be obtained by counting the trajectories of the angular velocity only.

Figure 3 shows the time series of ΔS_{tot} for the two cases, with Δt taking three representative values. For $\Delta t = 0.01$ s [Fig. 3(a)], the range of ΔS_{tot} is small, and the two entropy definitions agree with each other well. For $\Delta t = 0.04$ s [Fig. 3(b)], the range of ΔS_{tot} becomes larger, and the two entropy definitions still agree well, just occasionally, one can see the deviation between the two. For $\Delta t = 0.11$ s $\approx \tau$ [Fig. 3(c)], the agreement is reasonably well, where the deviation between $\Delta S_{\text{tot}}^{(\text{I})}$ and $\Delta S_{\text{tot}}^{(\text{II})}$ is noticeable, which can be attributed to the systematic deviation between the trajectory entropy and the environment entropy when $\Delta t \geqslant \tau$. Comparing ΔS_{tot} for different Δt, Figs. 3(a) and 3(b) share many common features regarding the most dominant peaks or dips, although the timescale in Fig. 3(b) is four times larger. Figure 3(c) is further coarse grained, that despite the slow varying trend, the sharp fluctuations in Figs. 3(a) and 3(b) are no longer noticeable.
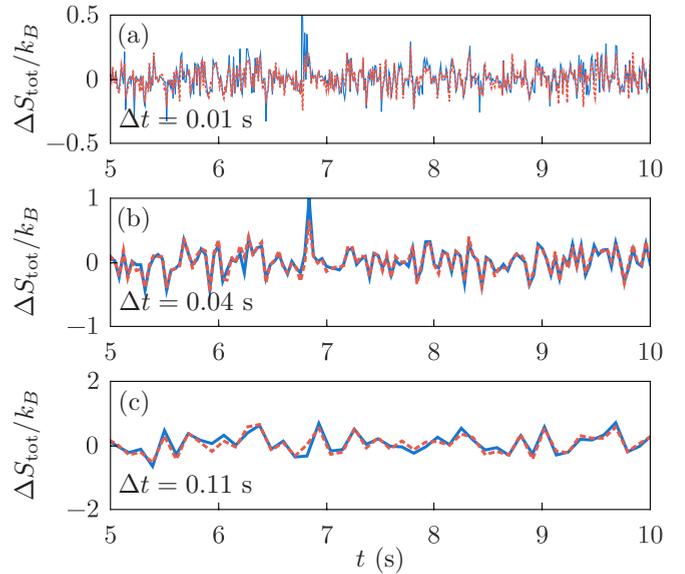

FIG. 3. [(a)–(c)] The time series of the total entropy production for different Δt. (a) $\Delta t = 0.01$ s, (b) $\Delta t = 0.04$ s, and (c) $\Delta t = 0.11$ s. The red dashed curve is $\Delta S_{\text{tot}}^{(\text{I})}$ [Eq. (13)]; the blue solid curve is $\Delta S_{\text{tot}}^{(\text{II})}$ [Eq. (16)].

C. The fluctuation theorem

The fluctuation theorem is a necessary condition for the statistics of infima [24]. Here we examine the fluctuation theorem Eq. (1) using the experimental data. The symmetry function $\text{Sym}(\Delta S) = \ln \frac{P(\Delta S)}{P(-\Delta S)}$ for the total entropy productions is shown in Fig. 4. It is apparent that when ΔS_{tot} is small, the symmetry function $\text{Sym}(\Delta S_{\text{tot}})$ equals to $\Delta S_{\text{tot}}/k_B$ for both the entropy production expressions, validating the fluctuation theorem for the asymmetric Brownian motor. This is in consistent with previous results in granular medium for the injected work [8], a vertically placed asymmetric rotor in a granular gas [9], and a frictional granular motor [12]. When $|\Delta S_{\text{tot}}|$ is large, the case for $\Delta t = 0.04$ s follows the diagonal line best. But in general, due to the deviation of the distribution of $\Delta S_{\text{tot}}^{(\text{II})}$ from the Gaussian form, the data points for $\Delta S_{\text{tot}}^{(\text{II})}$ deviates from the diagonal line (the formula). Since $\Delta S_{\text{tot}}^{(\text{I})}$ uses the solutions of the Fokker-Planck equation, its symmetry function follows the formula better than $\Delta S_{\text{tot}}^{(\text{II})}$, especially for large Δt values.
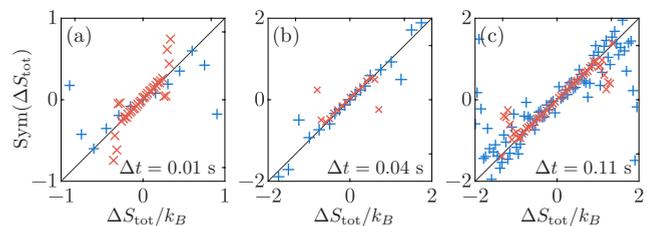

FIG. 4. The symmetry functions of the total entropy production for the asymmetric Brownian motor. From (a) to (c), $\Delta t = 0.01$ s, 0.04 s, and 0.11 s, respectively. Red crosses are for $\Delta S_{\text{tot}}^{(\text{I})}$, and blue pluses are for $\Delta S_{\text{tot}}^{(\text{II})}$.
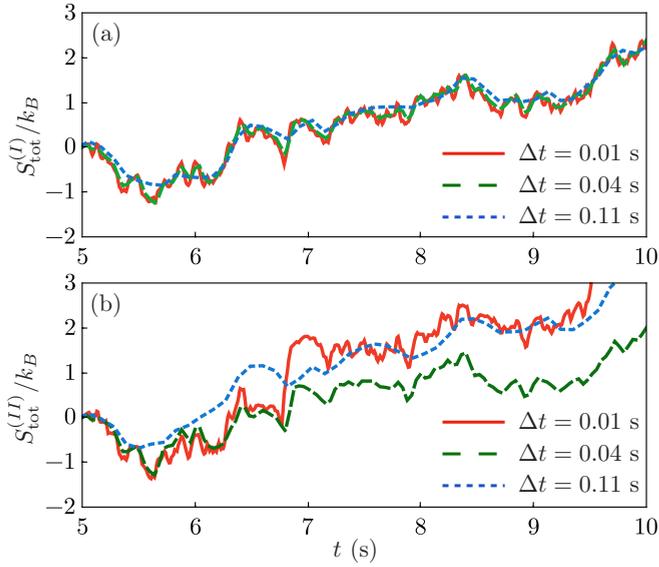
FIG. 5. The time dependence of the total entropy, with (a) for $S_{\text{tot}}^{(I)}(t)$ and (b) for $S_{\text{tot}}^{(II)}(t)$. For each case, three trajectories are shown: for $\Delta t = 0.01$ s (red solid curve), 0.04 s (green dashed curve), and 0.11 s (blue dotted curve).

The deviation of the data from the fluctuation theorem may be resulted from the limited data, nonidealities such as additional friction due to the ball-bearing, the effect of discontinuous collisions between the granular particle and the motor, etc. Since the fluctuation theorem is a necessary condition for the statistics of infima, the deviation may pose a question mark to the infima law, that for such nonideal small systems, will the infima law still hold?

IV. INFIMA STATISTICS OF THE TOTAL ENTROPY

In Ref. [24], by defining a minimum entropy in a time interval t_L, $S_{\text{inf}}(t_L) = \inf_{0 \leqslant t \leqslant t_L}[S_{\text{tot}}(t) - S_{\text{tot}}(0)]$, it has been found that the negative values of $S_{\text{inf}}(t_L)$ satisfy an exponential distribution in the $t_L \to \infty$ limit, i.e.,

$$P\big(S_{\text{inf}}^{\infty}\big) = \frac{1}{k_B} e^{S_{\text{inf}}^{\infty}/k_B}, \tag{17}$$

as a result, the average value of this negative entropy infimum over a large number of ensembles will be $-k_B$, $\langle S_{\text{inf}}^{\infty} \rangle = -k_B$. In general, for a finite time interval t_L, $\langle S_{\text{inf}}(t_L) \rangle > -k_B$. Thus $-k_B$ gives the lower bound of the average entropy infimum value.

In our case, the total entropy S_{tot} is an integration (summation) of the total entropy production ΔS_{tot}, e.g., Eq. (13) for $\Delta S_{\text{tot}}^{(I)}$ and Eq. (16) for $\Delta S_{\text{tot}}^{(II)}$. Figure 5 shows three segments of the time series $S_{\text{tot}}(t)$ with $\Delta t = 0.01$ s, 0.04 s, and 0.11 s, respectively. Although $\Delta S_{\text{tot}}^{(II)}$ and thus $S_{\text{tot}}^{(II)}$ is valid as far as $\Delta t \leqslant \tau \sim 0.112$ s (see Appendix B), it is clear that with a larger Δt, $S_{\text{tot}}(t)$ is coarse grained and loses the detailed fluctuations in the finer timescale, therefore may miss some of the dips in $S_{\text{tot}}(t)$ and yield a higher value of S_{inf}. Therefore, to identify the true infimum value, Δt should be as small as possible to avoid missing possible sharp dips in $S_{\text{tot}}(t)$. However, another condition requires $\Delta t \gg t_f = 0.002$ s, such that the observed transition between the angular velocities
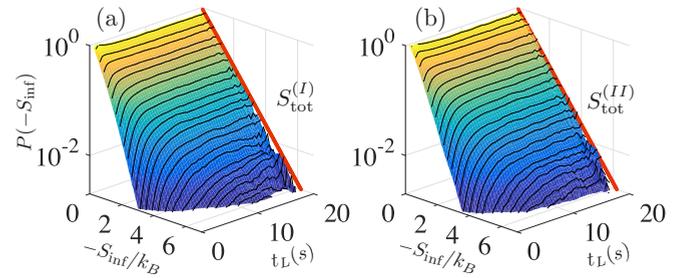

FIG. 6. The distribution of $S_{\text{inf}}(t_L)$ versus different t_L at $\Delta t = 0.01$ s. The distribution is window averaged with the width of the window in t_L being 0.5 s. The straight line is Eq. (17).

ω_i is a Markov process. Taking these considerations, we set $\Delta t = 0.01$ s in doing the statistics of infima (Appendix D).

For a given t_L that $t_L \gg \Delta t$, we can segregate the total five hours data of $S_{\text{tot}}^{(I)}(t)$ and $S_{\text{tot}}^{(II)}(t)$ into segments with length t_L, then for each segment, shift $S_{\text{tot}}(0)$ to 0, and count $S_{\text{inf}}(t_L) = \inf_{0 \leqslant t \leqslant t_L} S_{\text{tot}}(t)$. Therefore there will be (5 h/t_L) data points for each given t_L. Figure 6 shows the distribution of $S_{\text{inf}}(t_L)$ versus the variation of t_L. The distribution has an abrupt change around $t_L \sim 5$ s. For $t_L > 5$ s, the distribution of $S_{\text{inf}}(t_L)$ follows the exponential distribution well, i.e., in the log-linear scale it approximates a straight line, as indicated in Fig. 6. Furthermore, for a given t_L, the accumulative distribution of $S_{\text{inf}}(t_L)$ is bounded by $1 - e^{S_{\text{inf}}/k_B}$ [24], which has also been corroborated by the data.

The average value of $S_{\text{inf}}(t_L)$ versus t_L is plotted in Fig. 7 as the data points, and the solid curve is the window averaged result. It is clear that for most of the data, especially the window averaged value, $\langle S_{\text{inf}}(t_L) \rangle \geqslant -k_B$. Another observation is that $\langle S_{\text{inf}}(t_L) \rangle$ decreases fast for $0 < t_L < 5$ s, while it approaches a constant value around $t_L = 10$ s. This is consistent with the distribution plots shown in Fig. 6. To be concrete, we calculate the mean value of $S_{\text{inf}}(t_L)$ for t_L up to 20 s to get stable results,
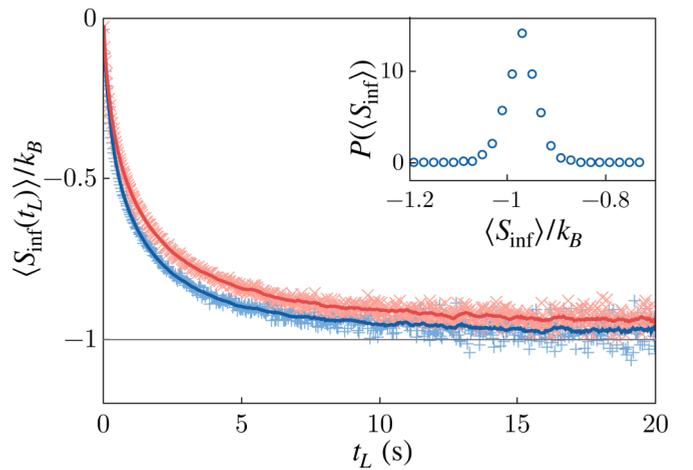

FIG. 7. The mean value of the infima $\langle S_{\text{inf}} \rangle$ versus t_L. The red crosses are for $S_{\text{tot}}^{(I)}$, and the blue pluses are for $S_{\text{tot}}^{(II)}$. The solid curves over the symbols are the window averaged value, with the width of the window in t_L being 0.5 s. The inset shows the distribution of $\langle S_{\text{inf}}(t_L) \rangle$ for $S_{\text{tot}}^{(II)}$ for $t_L \in [15, 20]$, where the mean value is $-0.97k_B$, and the standard deviation is $0.031k_B$.

yet t_L is not so large so the statistics are still reliable. Since $\langle S_{\text{inf}}(t_L) \rangle$ for $S_{\text{tot}}^{(\text{II})}$ has a lower value, and there are some data points fall below $-k_B$, it is necessary to do further statistics to examine whether $-k_B$ is a safe lower bound for $\langle S_{\text{inf}}(t_L) \rangle$. The inset shows the distribution of the data points of $\langle S_{\text{inf}}(t_L) \rangle$ for $S_{\text{tot}}^{(\text{II})}$ in the interval $t_L \in [15, 20]$. The mean value is $-0.97 k_B$, and the standard deviation is $0.031 k_B$, thus the infima law is in general satisfied. Furthermore, we have calculated $\langle S_{\text{inf}}(t_L) \rangle$ for a few points with much larger t_L, e.g., $t_L \sim 40$ s, which has almost the same mean values as that for $t_L = 20$ s. The results for a larger Δt, i.e., $\Delta t = 0.02$, 0.04 s are shown in Appendix E, which are consistent with the above analysis.

V. CONCLUSION

To conclude, we have experimentally investigated the entropy production in an underdamped Brownian motor. The equivalence of the trajectory entropy and the environment entropy have been demonstrated both theoretically and experimentally for two-step and multistep trajectories, where, in principal if the data is not limited, better agreement can be achieved for more steps. However, in realistic cases, due to the limitation of the amount of data, multistep trajectories lead to a reduced number of segments and thus less reliable statistics. Since in our case, only short time interval is needed, two-step trajectory entropy production is sufficient for obtaining concrete statistical results.

With both the environment entropy and the trajectory entropy, we have calculated the total entropy production using two expressions, one exploits the solutions of the Fokker-Plank equation with key parameters derived from the experiment, and the other counts only the trajectories of the angular velocity. By plotting the time series of the total entropy production ΔS_{tot} and the symmetry functions, we have demonstrated that the total entropy production calculated in these two ways agree with each other if the time interval Δt is small, and they both follow the fluctuation theorem reasonably well. But due to the nonidealities in the experiments, there are deviations from the fluctuation theorem when $|\Delta S_{\text{tot}}|$ is large. Since the fluctuation theorem is the condition for the process to be martingale, which further yields the infima law of the total entropy, it would be interesting to examine whether the infima law is still hold with the nonidealities in the experiments and the presence of deviations from the fluctuation theorem, in addition of the more complex under damped stochastic dynamics.

The time series of the total entropy $S_{\text{tot}}(t)$ is obtained by integrating the total entropy production ΔS_{tot}, then the infimum of the total entropy S_{inf} in a finite time interval t_L can be counted. For a given t_L, we have examined the distribution of S_{inf}, and found that when t_L is large, e.g., for t_L typically larger than 5 s, the data are well described by the exponential distribution $P(S_{\text{inf}}^{\infty}) = e^{S_{\text{inf}}^{\infty}/k_B}/k_B$, which has been proved to be valid when $t_L \to \infty$ [24]. The mean value of S_{inf}, in most cases, is larger than $-k_B$. The lowest value of $\langle S_{\text{inf}} \rangle$ occurs for $S_{\text{tot}}^{(\text{II})}$ when $\Delta t = 0.01$ s, where it fluctuates around $-k_B$. Further statistics for $\langle S_{\text{inf}} \rangle$ in the range $t_L \in [15, 20]$ s, where the value of $\langle S_{\text{inf}} \rangle$ is stabilized around $-k_B$, indicates a mean value of $-0.97 k_B$ with standard deviation $0.031 k_B$, which in
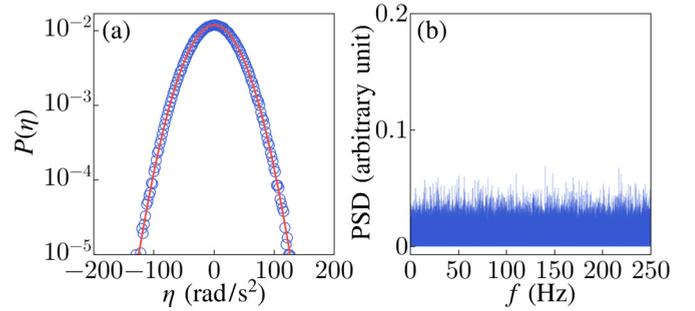

FIG. 8. The statistics of the effective noise $\eta(t)$ felt by the motor. (a) The distribution and (b) the power spectrum density (PSD).

principle stays inside the boundary set by the infima law of the total entropy [24].

As an experimentally tractable macroscopic system, the granular Brownian motor has been exploited specifically for the investigation of the nonequilibrium thermodynamics, particularly for the fluctuation theorem. Here using this system, we have verified the equivalence of the environment entropy and the trajectory entropy. By deriving the total entropy from the experimental data, we have verified the infima theorem about the infimum value of the entropy curve. Our results indicate that, although simple, the system can be a powerful apparatus in examining the theories developed in the nonequilibrium thermodynamics, especially for small systems.

APPENDIX A: STATISTICS OF THE EFFECTIVE NOISE

From the underdamped Langevin equation (3), the noise $\eta(t)$ can be solved out as

$$\eta(t) = -\frac{d}{dt}\omega(t) + \frac{\gamma}{I}\omega(t) - \frac{M}{I}.$$

After obtaining $\omega(t)$, $d\omega/dt$ can be approximated by $[\omega(t + t_f) - \omega(t)]/t_f$, then the noise $\eta(t)$ can be derived with the above equation from the measurements. Figure 8 plots the statistics of $\eta(t)$, which shows clearly that it is Gaussian white noise.

APPENDIX B: TWO-STEP TRAJECTORY ENTROPY

From the corresponding Fokker-Planck equation (8) of the Langevin equation (3), the forward and backward transition probability within the time duration Δt is given by

$$P(\omega_{i-1} \to \omega_i, \Delta t)$$
$$\propto \exp\left\{ -\frac{I[(\omega_i - \langle\omega\rangle) - (\omega_{i-1} - \langle\omega\rangle)e^{-\Delta t/\tau}]^2}{2k_B T(1 - e^{-2\Delta t/\tau})} \right\}, \quad \text{(B1)}$$
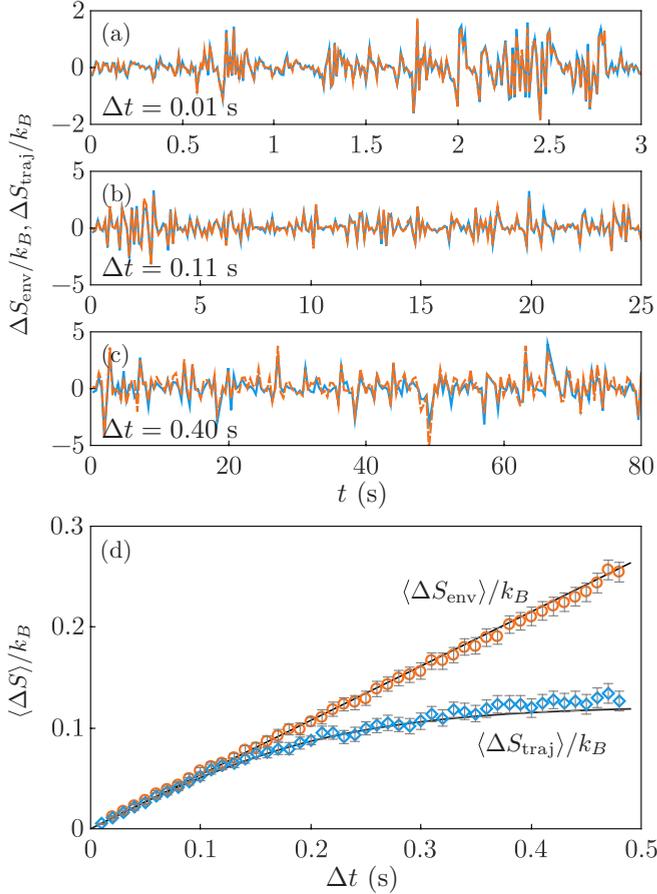
FIG. 9. [(a)–(c)] The entropy change versus time. Blue curves are for ΔS_{traj} and red curves are for ΔS_{env}. From (a) to (c) the sampling time interval $\Delta t = 0.01$ s, 0.11 s, and 0.40 s, respectively. (d) The mean environment and trajectory entropy as a function of sampling time interval Δt. The blue diamonds are for the mean trajectory entropy $\langle \Delta S_{\text{traj}} \rangle$, and the red circles are for the entropy change of the environment $\langle \Delta S_{\text{env}} \rangle$. The curves are the formula Eqs. (B4) and (B5).

$$P(-\omega_i \rightarrow -\omega_{i-1}, \Delta t)$$
$$\propto \exp\left\{ -\frac{I[(-\omega_{i-1} - \langle\omega\rangle) + (\omega_i + \langle\omega\rangle)e^{-\Delta t/\tau}]^2}{2k_B T (1 - e^{-2\Delta t/\tau})} \right\}. \tag{B2}$$

Substituting back to Eq. (15), and after some algebra, one gets:

$$\Delta S_{\text{traj}}^{(2)} = \frac{-I(\omega_i^2 - \omega_{i-1}^2)}{2T} + \frac{M(\omega_i + \omega_{i-1})\tau}{T}\frac{1 - e^{-\Delta t/\tau}}{1 + e^{-\Delta t/\tau}}. \tag{B3}$$

For $\Delta t \rightarrow 0$, the factor $(1 - e^{-\Delta t/\tau})/(1 + e^{-\Delta t/\tau})$ can be approximated by $\Delta t/(2\tau)$, then the second term becomes $M(\omega_i + \omega_{i-1})\Delta t/(2T) = M\Delta\theta$, which is the approximated work injected into the Brownian motor. Therefore, in this limit, and given that Eqs. (B1) and (B2) are still valid for the data, we have $\Delta S_{\text{traj}}^{(2)} \approx \Delta S_{\text{env}}$ [21].

Figures 9(a)–9(c) show $\Delta S_{\text{traj}}^{(2)}$ and ΔS_{env} together versus time t for $\Delta t = 0.01$, 0.11, and 0.4 s, respectively. Note that the characteristic correlation time of the system is

$\tau = 0.112$ s. It is clear that when Δt is large, e.g., 0.4 s, the deviation between $\Delta S_{\text{traj}}^{(2)}$ and ΔS_{env} is obvious due to the factor $(1 - e^{-\Delta t/\tau})/(1 + e^{-\Delta t/\tau})$, which is approximately $0.53\Delta t/(2\tau)$. As Δt becomes smaller, the effect of the factor $(1 - e^{-\Delta t/\tau})/(1 + e^{-\Delta t/\tau})$ becomes smaller, as it approximates $\Delta t/(2\tau)$ better. For example, it equals to $0.914\Delta t/(2\tau)$ and $0.999\Delta t/(2\tau)$ for $\Delta t = 0.11$ s and 0.01 s, respectively. In these cases, the two curves agree well.

Figure 9(d) plots the average value of $\Delta S_{\text{traj}}^{(2)}$ and ΔS_{env} versus Δt. $\langle \Delta S_{\text{env}} \rangle$ increases with Δt linearly. This is because as the system is in a steady state, $\langle \Delta E_k \rangle = 0$, thus

$$\langle \Delta S_{\text{env}} \rangle = \langle \Delta W \rangle / T = M\langle\omega\rangle \Delta t / T. \tag{B4}$$

While for $\langle \Delta S_{\text{traj}}^{(2)} \rangle$, from Eq. (B3), since $\langle \omega_i^2 \rangle = \langle \omega_{i-1}^2 \rangle$, and $\langle \omega_i + \omega_{i-1} \rangle = 2\langle\omega\rangle$, we have

$$\langle \Delta S_{\text{traj}}^{(2)} \rangle = M\langle\omega\rangle \left[2\tau \frac{1 - e^{-\Delta t/\tau}}{1 + e^{-\Delta t/\tau}} \right] / T. \tag{B5}$$

Therefore when $\Delta t \ll \tau$, $\langle \Delta S_{\text{traj}}^{(2)} \rangle \approx \langle \Delta S_{\text{env}} \rangle$. When $\Delta t \gg \tau$, their difference will be significant. These equations are shown in Fig. 9(d) as the curves.

Similar results have been found in circuit experiments [21], where $\Delta S_{\text{traj}}^{(2)} \approx \Delta S_{\text{env}}$ was observed in the $\Delta t \rightarrow 0$ case. The circuit system in a constant heat reservoir follows the Langevin equation. However, the granular Brownian motor experiment does not strictly follow the ideal Langevin dynamics due to the friction of the ball-bearing (although it is small). In addition, the Gaussian noise $\eta(t)$ in the ideal Langevin dynamics is continuous. But in granular systems, the noise is generated from the collisions of the granular particles to the Brownian motor, which can be regarded as a continuous process only when the coarse-graining time unit is large enough. Nevertheless, our experimental results provide direct evidence for the equivalence of the environment entropy and the two-step trajectory entropy for a Brownian motor in granular gases under certain conditions.

APPENDIX C: MULTISTEP TRAJECTORY ENTROPY

The above subsection has considered the trajectory entropy production for two-step trajectories (including only one Δt in every trajectory), and measured the trajectory entropy with different time interval Δt. Here we shall calculate multistep trajectory entropy, and demonstrate that how the trajectory entropy $\Delta S_{\text{traj}}^{(n)}$ and the environmental entropy ΔS_{env} are equivalent in the short time limit.

According to Eq. (15), the three-step trajectory entropy can be expressed as:

$$\Delta S_{\text{traj}}^{(3)} = k_B \ln \frac{P(\omega_2|\omega_1)P(\omega_1|\omega_0)}{P(-\omega_0|-\omega_1)P(-\omega_1|-\omega_2)}$$
$$= k_B \ln \frac{P(\omega_2|\omega_1)}{P(-\omega_1|-\omega_2)} + k_B \ln \frac{P(\omega_1|\omega_0)}{P(-\omega_0|-\omega_1)}, \tag{C1}$$

where ω_i is the ith step angular velocity in a trajectory, and the time interval between two adjacent steps is Δt. The $(n+1)$-step trajectory contains n time intervals. Equation (C1) also gives the relation of the multistep trajectory entropy and the two-step trajectory entropy: $\Delta S_{\text{traj}}^{(3)} = \Delta S_{\text{traj}}^{(2)}(t_0 \rightarrow t_1) + \Delta S_{\text{traj}}^{(2)}(t_1 \rightarrow t_2)$, which is natural as the total entropy produc-

tion is an additive quantity. Substituting Eq. (B3) to Eq. (C1), we can obtain:

$$\Delta S_{\text{traj}}^{(3)} = -\frac{I}{2T}\big(\omega_i^2 - \omega_{i-2}^2\big)$$
$$+ \frac{M(\omega_i + 2\omega_{i-1} + \omega_{i-2})\tau}{T}\frac{1 - e^{-\Delta t/\tau}}{1 + e^{-\Delta t/\tau}}, \quad \text{(C2)}$$

and the $(n + 1)$-step trajectory entropy change is

$$\Delta S_{\text{traj}}^{(n+1)} = -\frac{I}{2T}\big(\omega_i^2 - \omega_{i-n}^2\big) + \frac{1 - e^{-\Delta t'/n\tau}}{1 + e^{-\Delta t'/n\tau}}$$
$$\times \frac{M[\omega_i + 2(\omega_{i-1} + \cdots + \omega_{i-n+1}) + \omega_{i-n}]\tau}{T}.$$
$$\text{(C3)}$$

The new time interval $\Delta t' = n\Delta t$ is used in this equation, which is the total length of the trajectory, i.e., $\Delta t' = 2\Delta t$ in the case of three-step trajectory. Taking average of Eq. (C3) and using $\langle\omega_i + \omega_{i-1}\rangle = 2\langle\omega\rangle$, the average entropy production of multistep trajectories can be obtained as

$$\big\langle\Delta S_{\text{traj}}^{(n+1)}\big\rangle = -\Big\langle\frac{\Delta Q}{T}\Big\rangle + \frac{M}{T}2n\langle\omega\rangle\tau\frac{1 - e^{-\Delta t'/(n\tau)}}{1 + e^{-\Delta t'/(n\tau)}}. \quad \text{(C4)}$$

Note that $\langle-\Delta Q/T\rangle = 0$. The Taylor expansion of the second part in Eq. (C4) yields:

$$\big\langle\Delta S_{\text{traj}}^{(n+1)}\big\rangle = \frac{M}{T}2n\langle\omega\rangle\tau\left[\frac{\frac{\Delta t'}{n\tau} - \frac{(\Delta t')^2}{2(n\tau)^2} + O(\Delta t'^3)}{1 + 1 - \frac{\Delta t'}{n\tau} + \frac{(\Delta t')^2}{2(n\tau)^2} + O(\Delta t'^3)}\right]$$
$$\approx \frac{M}{T}\langle\omega\rangle\Delta t'\left(1 - \frac{\Delta t'}{2n\tau}\right). \quad \text{(C5)}$$

Equation (C5) gives the ensemble average of the multistep trajectory entropy production $\langle\Delta S_{\text{traj}}^{(n+1)}\rangle$. Comparing with the environmental thermal entropy production $\frac{M}{T}\langle\omega\rangle\Delta t'$ [Eq. (B4)] with trajectory length $\Delta t'$, the difference is given by $-\frac{\Delta t'}{2n\tau}$. Therefore for a fixed total time interval $\Delta t'$, the difference between the trajectory entropy and the environmental entropy productions decreases as the number of steps in the trajectory becomes larger. In particular, in the large n limit, $\Delta t' \ll 2n\tau$, the two should coincide with each other. Therefore, theoretically the trajectory entropy would be equal to the environmental thermal entropy in the continuous-time (large n) limit.

This relation can be verified experimentally. Limited by the total number of samples, when we use multistep trajectories, we need to make ω_{bin} larger to ensure that most trajectories have corresponding reverse trajectories. To be practical, we set $\omega_{\text{bin}} = 0.15$ rad/s for three-step trajectories, and $\omega_{\text{bin}} = 0.2$ rad/s for four-step trajectories. After enlarging ω_{bin}, more than 95% of the reverse trajectories can be found for the three- and four-step trajectories.

The multistep trajectory entropy productions are plotted in Fig. 10. In principle, with the increase of the number of steps n, counting trajectories would become a more accurate way of measuring entropy production [see Eq. (C5)]. This is indeed the case for the average entropy production, as can be seen clearly from Figs. 10(g) and 10(h), especially comparing with Fig. 9(d). To be specific, in Fig. 9(d), for $n = 2$, the deviation occurs around Δt or $\Delta t'$ equals to $\tau = 0.112$ s. In
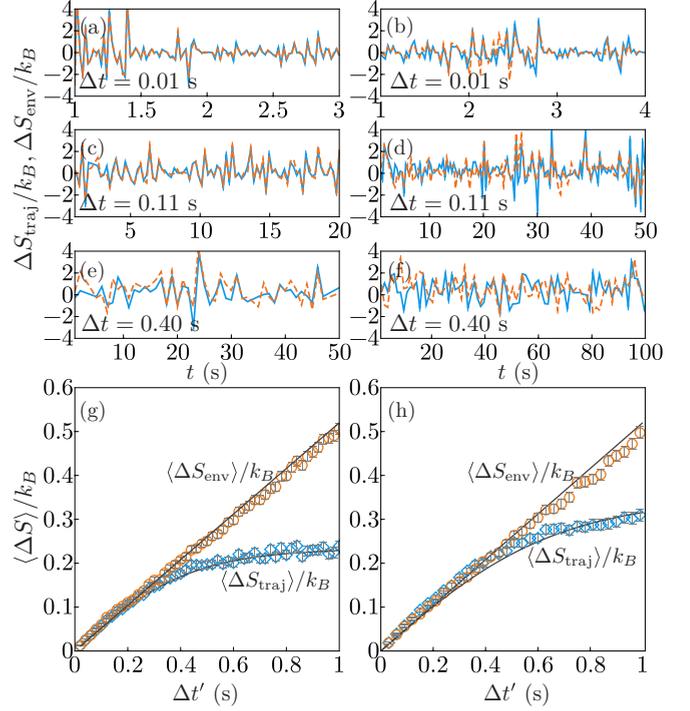

FIG. 10. [(a)–(f)] The time series of ΔS_{traj} and ΔS_{env}. The red curves are $\Delta S_{\text{env}}(t)$ and the blue curves are ΔS_{traj}. [(g) and (h)] The mean trajectory and environment entropy change as a function of $\Delta t'$. Red circles are $\langle\Delta S_{\text{env}}\rangle$ and blue diamonds are ΔS_{traj}. The left panels are for three-step trajectory entropy production, where $\Delta t' = 2\Delta t$, and the right panels are for four-step trajectory entropy production with $\Delta t' = 3\Delta t$.

Fig. 10(g), for $n = 3$, the deviation starts around $\Delta t' \sim 0.3$ s, while in Fig. 10(h) for $n = 4$, the deviation starts around $\Delta t' \sim 0.4$ s. But for the entropy production versus time, as the number of steps n increases, even by increasing the value of $\Delta\omega$, due to the limited data, the statistics of the reverse trajectories deteriorates. Thus S_{traj} deviates from S_{env}, and the deviation becomes more obvious as Δt gets larger or n is larger, as demonstrated in Figs. 10(a)–10(f). Therefore to obtain reliable results, a trade-off due to different effects needs to be considered in dealing with the experimental data.

APPENDIX D: VERIFICATION AND CONDITION OF MARKOV PROCESS

To verify that the motion of the motor is a Markov process and to examine its condition, we plot the joint probability distribution of $P(\omega_{i+2}|\omega_{i+1}, \omega_i)$ and $P(\omega_{i+2}|\omega_{i+1})$ for the measured angular velocity time series in Fig. 11. If $\{\omega_i\}$ is a Markov process, then the probability of $P(\omega_{i+2}|\omega_{i+1}, \omega_i)$ will be the same as $P(\omega_{i+2}|\omega_{i+1})$, i.e., the current state only depends on the previous one-step state. This will result in a distribution along the diagonal line in the plot. Note that the time interval between two adjacent frames is $t_f = 0.002$ s. From the results shown in Fig. 11, when Δt is too small, e.g., $\Delta t = 0.004$ s, although the joint probability takes high values along the diagonal line, the distribution is broad, indicating the influence of ω_i to ω_{i+2}. As Δt becomes larger, the distribution
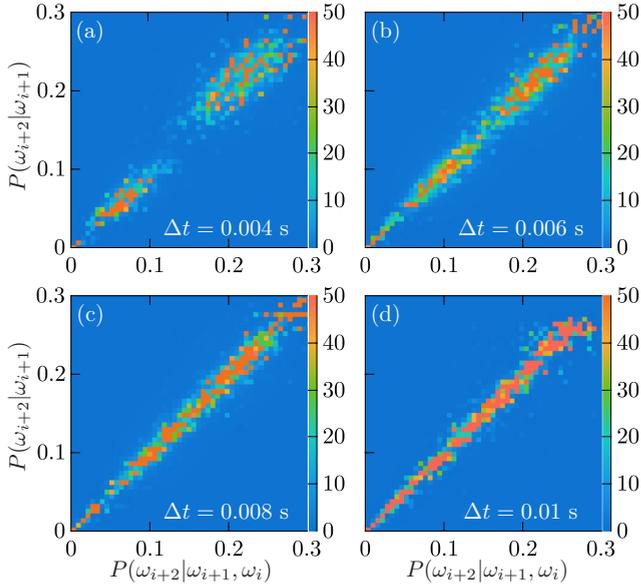
FIG. 11. The joint probability distribution of $P(\omega_{i+2}|\omega_{i+1},\omega_i)$ and $P(\omega_{i+2}|\omega_{i+1})$. [(a)–(d)] are for $\Delta t = 0.004$ s, 0.006 s, 0.008 s, and 0.01 s, respectively. $t_f = 0.002$ s.

becomes narrower, and for $\Delta t = 0.01$ s, the distribution is mostly focused on the diagonal line, verifying the Markov process. Thus in our calculation, we will choose $\Delta t \geqslant 0.01$ s to guarantee that the Markov process condition is fulfilled.

APPENDIX E: STATISTICS OF INFIMA FOR $\Delta t > 0.01$ s AND THE EFFECT OF DIFFERENT COARSE-GRAINING BINS

For $\Delta t = 0.04$ s, especially for large t_L, the distribution is not so smooth and deviates slightly from the exponential distribution (Fig. 12). For $t_L < 5$ s, for all the Δt values, the deviation of the distribution of $S_{\inf}(t_L)$ from the exponential distribution is apparent.

For the average value of the infimum, a general trend is that as Δt becomes larger, $\langle S_{\inf}(t_L) \rangle$ also gets larger, as demonstrated in Fig. 13, due to the coarse-graining effect as discussed in the main text. Furthermore, as the total length of the data is fixed, for larger t_L, the number of segments becomes smaller, resulting in deteriorated statistics.
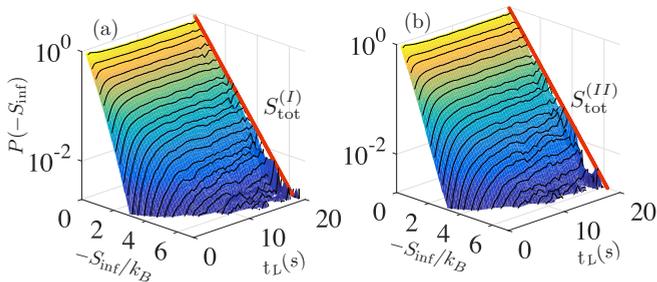

FIG. 12. The distribution of $S_{\inf}(t_L)$ versus different t_L for $\Delta t = 0.04$ s. The distribution is window averaged with the width of the window in t_L being 0.5 s. The straight line is Eq. (17).
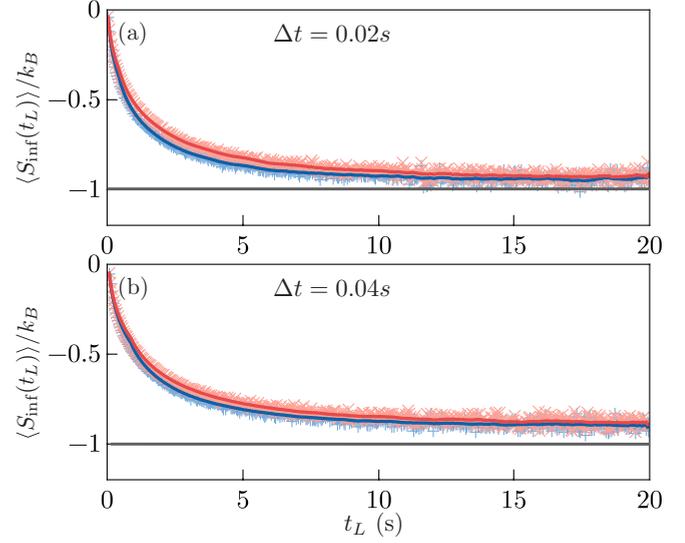

FIG. 13. The mean value of the infimum $\langle S_{\inf} \rangle$ versus (t_L). The red crosses are for $S_{\text{tot}}^{(I)}$, and the blue pluses are for $S_{\text{tot}}^{(II)}$. The solid curves over the symbols are the window averaged value, with the width of the window in t_L being 0.5 s. Panels (a) and (b) are for $\Delta t = 0.02$ s, and 0.04 s, respectively. The step in t_L is the corresponding Δt.

Another technical detail is to choose the size of the bin in the coarse-graining process of the angular velocity ω properly. This is because if the bin is too small, it will decrease the number of corresponding reverse trajectories or even lead to no reverse trajectories for a considerable amount of forward trajectories, rendering unreliable statistics. While if the bin
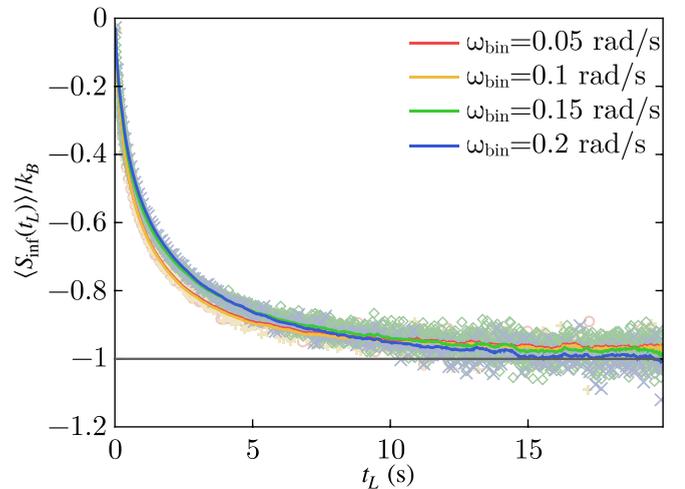

FIG. 14. The infimum of $S_{\text{tot}}^{(II)}$ for $\Delta t = 0.01$ s. Red circles are for $\omega_{\text{bin}} = 0.05$ rad/s, yellow pluses for $\omega_{\text{bin}} = 0.1$ rad/s, green diamonds for $\omega_{\text{bin}} = 0.15$ rad/s, and blue crosses for $\omega_{\text{bin}} = 0.2$ rad/s. The solid curves are the window averaged value with a window size of 0.5 s in t_L. For t_L around 15 s, the four curves from top to down are for $\omega_{\text{bin}} = 0.05$, 0.1, 0.15, and 0.2 rad/s, respectively. While for t_L around 3 s, the order is reversed. For every selected ω_{bin}, there is a small fraction (f) of the forward trajectories that have no corresponding backward trajectories: $f = 2.0\%$, 0.9%, 0.02%, and 0.01% for $\omega_{\text{bin}} = 0.05$, 0.1, 0.15, and 0.2 rad/s, respectively.

is too large, it will lose much of the details of the angular velocities and may result in inaccurate results. However, the results should be not so sensitive, that there should be a range for the size of the bin where the results are stable. To be specific, we have in addition checked different sizes of the bin, e.g., with $\omega_{bin} = 0.05, \ 0.15, \ \text{and} \ 0.2$ rad/s. The results, together with that $\omega_{bin} = 0.1$ rad/s, are shown in Fig. 14. It is clear that within this range, the results are relatively stable.

[1] T. L. Hill, *Thermodynamics of Small Systems* (Courier Corporation, London, 1994).

[2] D. J. Evans, E. G. D. Cohen, and G. P. Morriss, Phys. Rev. Lett. **71**, 2401 (1993).

[3] D. J. Evans and D. J. Searles, Phys. Rev. E **50**, 1645 (1994).

[4] J. Kurchan, J. Phys. A **31**, 3719 (1998).

[5] G. E. Crooks, Phys. Rev. E **60**, 2721 (1999).

[6] D. J. Evans and D. J. Searles, Adv. Phys. **51**, 1529 (2002).

[7] Y.-J. Yang and H. Qian, Phys. Rev. E **101**, 022129 (2020).

[8] K. Feitosa and N. Menon, Phys. Rev. Lett. **92**, 164301 (2004).

[9] S. Joubaud, D. Lohse, and D. vanderMeer, Phys. Rev. Lett. **108**, 210604 (2012).

[10] A. Naert, Europhys. Lett. **97**, 20010 (2012).

[11] A. Gnoli, A. Petri, F. Dalton, G. Pontuale, G. Gradenigo, A. Sarracino, and A. Puglisi, Phys. Rev. Lett. **110**, 120601 (2013).

[12] A. Gnoli, A. Sarracino, A. Puglisi, and A. Petri, Phys. Rev. E **87**, 052209 (2013).

[13] A. Gnoli, A. Puglisi, and H. Touchette, Europhys. Lett. **102**, 14002 (2013).

[14] F. Douarche, S. Joubaud, N. B. Garnier, A. Petrosyan, and S. Ciliberto, Phys. Rev. Lett. **97**, 140603 (2006).

[15] S. Ciliberto, S. Joubaud, and A. Petrosyan, J. Stat. Mech.: Theory Exp. (2010) P12003.

[16] G. M. Wang, E. M. Sevick, E. Mittag, D. J. Searles, and D. J. Evans, Phys. Rev. Lett. **89**, 050601 (2002).

[17] D. M. Carberry, J. C. Reid, G. M. Wang, E. M. Sevick, D. J. Searles, and D. J. Evans, Phys. Rev. Lett. **92**, 140601 (2004).

[18] O.-P. Saira, Y. Yoon, T. Tanttu, M. Möttönen, D. V. Averin, and J. P. Pekola, Phys. Rev. Lett. **109**, 180601 (2012).

[19] K.-H. Chiang, C.-W. Chou, C.-L. Lee, P.-Y. Lai, and Y.-F. Chen, Europhys. Lett. **113**, 30001 (2016).

[20] K.-H. Chiang, C.-L. Lee, P.-Y. Lai, and Y.-F. Chen, Phys. Rev. E **96**, 032123 (2017).

[21] K.-H. Chiang, C.-L. Lee, P.-Y. Lai, and Y.-F. Chen, Phys. Rev. E **95**, 012158 (2017).

[22] D. Collin, F. Ritort, C. Jarzynski, S. B. Smith, I. Tinoco Jr, and C. Bustamante, Nature **437**, 231 (2005).

[23] M. Rossi, L. Mancino, G. T. Landi, M. Paternostro, A. Schliesser, and A. Belenchia, Phys. Rev. Lett. **125**, 080601 (2020).

[24] I. Neri, É. Roldán, and F. Jülicher, Phys. Rev. X **7**, 011019 (2017).

[25] S. Singh, É. Roldán, I. Neri, I. M. Khaymovich, D. S. Golubev, V. F. Maisi, J. T. Peltonen, F. Jülicher, and J. P. Pekola, Phys. Rev. B **99**, 115422 (2019).

[26] S. Pigolotti, I. Neri, É. Roldán, and F. Jülicher, Phys. Rev. Lett. **119**, 140604 (2017).

[27] F. Jülicher, A. Ajdari, and J. Prost, Rev. Mod. Phys. **69**, 1269 (1997).

[28] U. Seifert, Phys. Rev. Lett. **95**, 040602 (2005).

[29] R. van Zon and E. G. D. Cohen, Phys. Rev. Lett. **91**, 110601 (2003).

[30] A. Gomez-Marin and I. Pagonabarraga, Phys. Rev. E **74**, 061113 (2006).

[31] S. Regev and O. Farago, Physica **507**, 231 (2018).

[32] B. Cleuren and R. Eichhorn, J. Stat. Mech.: Theory Exp. (2008) P10011.

[33] M. van den Broek and C. Van den Broeck, Phys. Rev. E **78**, 011102 (2008).

[34] G. Costantini, A. Puglisi, and U. M. B. Marconi, Eur. Phys. J.: Spec. Top. **179**, 197 (2009).

[35] P. Eshuis, K. van der Weele, D. Lohse, and D. van der Meer, Phys. Rev. Lett. **104**, 248001 (2010).

[36] R. Balzan, F. Dalton, V. Loreto, A. Petri, and G. Pontuale, Phys. Rev. E **83**, 031310 (2011).

[37] J. Talbot, R. D. Wildman, and P. Viot, Phys. Rev. Lett. **107**, 138001 (2011).

[38] L. O. Gálvez and D. van der Meer, J. Stat. Mech.: Theory Exp. (2016) 043206.

[39] https://imagej.nih.gov/ij/index.html.

[40] H. Nyquist, Phys. Rev. **32**, 110 (1928).

[41] R. Kubo, Rep. Prog. Phys. **29**, 255 (1966).

[42] A different approach to estimate the correlation time is to find the breakpoint of the power spectrum of ω [9], yielding $\tau = 0.122$ s, agrees reasonably well with that obtained from the correlation function.

[43] A. Imparato and L. Peliti, Phys. Rev. E **74**, 026106 (2006).